




## RESEARCH ARTICLE

WILEY

# Melanoma segmentation: A framework of improved DenseNet77 and UNET convolutional neural network

Marriam Nawaz<sup>1,7</sup> | Tahira Nazir<sup>2</sup> | Momina Masood<sup>1</sup>  | Farooq Ali<sup>1</sup> |  
Muhammad Attique Khan<sup>3</sup>  | Usman Tariq<sup>4</sup> | Naveera Sahar<sup>5</sup> |  
Robertas Damaševičius<sup>6</sup> 

<sup>1</sup>Department of Computer Science,  
University of Engineering and  
Technology, Taxila, Pakistan

<sup>2</sup>Department of Computing, Riphah  
International University, Islamabad,  
Pakistan

<sup>3</sup>Department of Computer Science,  
HITEC University Taxila, Taxila, Pakistan

<sup>4</sup>College of Computer Engineering and  
Science, Prince Sattam Bin Abdulaziz  
University, Al-Kharj, Saudi Arabia

<sup>5</sup>Department of Computer Science,  
University of Wah, Wah Cantt, Pakistan

<sup>6</sup>Faculty of Applied Mathematics, Silesian  
University of Technology, Gliwice, Poland

<sup>7</sup>Department of Software Engineering,  
University of Engineering and Technology,  
Taxila, Pakistan

## Correspondence

Muhammad Attique Khan, Department of  
Computer Science, HITEC University  
Taxila, Taxila, 47080, Pakistan.  
Email: [attique.khan@hitecuni.edu.pk](mailto:attique.khan@hitecuni.edu.pk)

## Abstract

Melanoma is the most fatal type of skin cancer which can cause the death of victims at the advanced stage. Extensive work has been presented by the researcher on computer vision for skin lesion localization. However, correct and effective melanoma segmentation is still a tough job because of the extensive variations found in the shape, color, and sizes of skin moles. Moreover, the presence of light and brightness variations further complicates the segmentation task. We have presented improved deep learning (DL)-based approach, namely, the DenseNet77-based UNET model. More clearly, we have introduced the DenseNet77 network at the encoder unit of the UNET approach to computing the more representative set of image features. The calculated keypoints are later segmented by the decoder of the UNET model. We have used two standard datasets, namely, the ISIC-2017 and ISIC-2018 to evaluate the performance of the proposed approach and acquired the segmentation accuracies of 99.21% and 99.51% for the ISIC-2017 and ISIC-2018 datasets, respectively. We have confirmed through both the quantitative and qualitative results that the proposed improved UNET approach is robust to skin lesions segmentation and can accurately recognize the moles of varying colors and sizes.

## KEYWORDS

deep learning, DenseNet, dermoscopy, melanoma, skin moles, UNET

## 1 | INTRODUCTION

Skin cancer is the irregular development of skin cells in the human body, which are of three types, that is, melanoma, basal and squamous cell carcinoma.<sup>1</sup> The most serious and proliferative type of skin cancer is melanoma, which grows in the cells named melanocytes. According to the report,<sup>2</sup> there are approximately 10 000 deaths in the US because of this deadly skin disease. Melanoma is instigated by the irregular growth of skin particles which

in turn generate abnormal body moles which vary in texture, color, and size. The abnormal mole has a size above 6 mm with unusual colors, for example, brown, black, red, and pink, which needs a checkup by the expert. There are two severity levels of melanoma, namely, Benign and Malignant. Benign is the early stage of melanoma which can easily be treatable, while Malignant is the proliferative type of melanoma that can lead to death if left untreated. Primarily, dermatologists perform manual examinations of the melanoma moles by analyzing

their color, texture, and size. However, this manual procedure becomes slow due to the inadequate availability of skin experts. The recognition of melanoma at the initial level is essential as not only does it reduce the death rate but can also protect them from complex surgeries. Currently, artificial intelligence (AI) methods have averaged investigators or scientists to build valuable and automated methods for the recognition of melanoma.

Melanoma is identified through different approaches of AI which can be divided into machine learning (ML) and deep learning (DL) based techniques. The ML-based methods use handcrafted keypoints extraction approaches to recognize the melanoma lesions. However, existing ML-based approaches are incapable of perfectly diagnosing melanoma lesions due to different variations like size, color, and texture. To improve the performance of the diagnosis system, classification is accomplished after the segmentation process from normal skin, as done by the experts. The segmentation methods are utilized in References 3 and 4 for melanoma region identification, which gives a good description of the melanoma regions during keypoints calculation and accurate classification of affected portions. So, we can say that accurate segmentation is an essential step for the development of effective recognition systems. However, the performance of the region segmentation methods lowers considerably in the case of low-resolution images, low illumination conditions, variations in contrast, and chrominance. In real-world scenarios, it is practically hard to acquire images with unvarying characteristics, so there is a need for such a system that can overcome the above-stated challenges.

Nowadays different DL-based approaches are presented in the medical field for the diagnosis of several diseases from images like brain tumor detection,<sup>5</sup> eye disease identification,<sup>6</sup> lung cancer,<sup>7</sup> skin cancer detection,<sup>8</sup> etc. The capability of DL-based approaches in quantifying uncertainty in medical case studies has enabled them to better recognize the diseased areas of the human body.<sup>9–16</sup> In DL, a convolutional neural network (CNN) is utilized for feature extraction from images and gives a better solution for melanoma regions from skin images. According to the existing research, DL plays an important role in the recognition of melanoma and has fascinated the investigator's attention. However, these approaches necessitate preprocessing procedures to overwhelm the issue of feature map saturation.<sup>17</sup> To overcome such problems, some approaches employing the mapping of the images into pixel-wise labels through the keypoints learning procedure are introduced by the researchers<sup>18,19</sup>; however, still there is a need for performance improvement.

Accurately and timely recognition and classification of melanoma in different varying conditions is still a

challenge in the field of medical imaging. Moreover, the occurrence of various artifacts like hair and tiny blood vessels further complicates the lesion segmentation process. To reduce the limitations of existing approaches, we have presented the DL-based technique, namely, DenseNet77-based UNET. More specifically, we have introduced DenseNet77 at the encoder part of the UNET approach to computing the deep features from the suspected samples. The calculated features are later used to be classified by the UNET decoder. The presented approach has the following main contributions:

- Presented improved UNET approach with DenseNet-77 for keypoints extraction, which improved the segmentation power in identifying small lesions while minimizing both training and testing time complexity.
- Effective skin lesions segmentation performance due to the robust feature computation power of the modified UNET approach.
- Presents such an approach that can locate the diseased portion even under the existence of noise, blurring, color, size, and slight alterations due to the efficient feature computation power of the DenseNet-77-based UNET framework.
- Better melanoma lesion recognition power of the proposed approach due to the ability of the DenseNet77-based UNET approach to tackle the over-fitted model data.
- Extensive experimentations have been performed over the challenging datasets, namely, ISIC-2017 and ISIC-2018 and have confirmed that the proposed solution is robust to skin cancer moles segmentation.

The remaining manuscript follows the following structure: the related work from history is depicted in Section 2, while the introduced approach is discussed in Section 3. We have defined the datasets along with the obtained results in Section 4, while the conclusion is given in Section 5.

## 2 | RELATED WORK

A detailed review of existing melanoma detection methods was conducted and the outcomes of all relevant studies are summarized in this section. Numerous ML approaches have been introduced for the automated diagnosis of melanoma. Several automated and semi-automated melanoma-specific attribute computation and classification approaches have been developed for processing dermoscopic images. Alquran et al.<sup>20</sup> proposed a method based on hand-crafted features. Initially, preprocessing and segmentation were performed to

extract the lesion area. Then, the gray level co-occurrence matrix and ABCD rule<sup>21</sup> were used to compute the keypoints. Then, the support vector machine (SVM) classifier was trained using extracted keypoints and classified the data into normal or melanoma affected. The results indicate that the categorization was 92.1% accurate. Codella et al.<sup>22</sup> proposed an ensemble method for melanoma detection. First, melanoma lesion region segmentation was performed using the UNET architecture, and then various features, including hand-coded, sparse-coding, and deep features, were extracted from both the segmented and the entire dermoscopic image. Then, the SVM classifier was trained individually over each feature vector, and the final disease confidence score was obtained by averaging their output. This method<sup>22</sup> attained an accuracy of 76% and requires performance improvement. Daghrir et al.<sup>23</sup> suggested a hybrid approach for the classification of melanoma lesions. The input image was preprocessed and segmented using derivatives of the Gaussian filter and the Otsu method, respectively. The scale-invariant feature transform (SIFT) and histogram of oriented gradients were used to determine the representative features and classified using the SVM and k-nearest neighbor (KNN) to categorize the melanoma moles. The authors also proposed a custom CNN comprising nine layers to compute deep features. The final results were obtained by aggregating the output of these approaches using a majority vote method. This system<sup>23</sup> produces better melanoma detection accuracy; however, it needs extensive training. Bama et al.<sup>24</sup> presented a method for segmenting the melanoma area based on superpixel region growth. The method was based on the Gaussian Mixture Model (GMM) which accurately partitions the candidate image into homogeneous sections. The melanoma area is then segregated by giving color labels to each of the superpixels computed with the delta metric which can identify extremely subtle color differences that human eyes cannot perceive. This approach<sup>24</sup> showed a segmentation accuracy of 86.83% on the PH2 database; however, the performance requires further improvement. Hu et al.<sup>25</sup> proposed a codeword learning method based on a feature similarity measure for categorizing melanoma into benign or malignant classes. Firstly, a combination of linearly independent and linear prediction (LP) approaches was used to compute correlated features. Then, the representative feature set was obtained using the RGB color histogram and SIFT descriptor. The obtained keypoint vectors were used to train an SVM classifier and perform classification. This approach<sup>25</sup> efficiently uses computing resources; however, the performance depends on the size of the codebook.

Recently, the DL and CNN methods are receiving increasing attention because of their improved and

accurate results. These methods are also being used by researchers in the field of medical imaging that aid radiologists and dermatologists in diagnosing severe illnesses more rapidly. Ameri<sup>26</sup> developed a lightweight model for the self-diagnosis of skin lesions that can be used on smartphones. A pre-trained CNN model based on AlexNet was used and fine-tuned on the HAM10000 database for the melanoma lesion categorization. This method<sup>26</sup> achieved an accuracy of 84%; however, the performance can be improved by employing large and diverse training sets. The region of interest (ROI) in a dermoscopic image was automatically extracted. Jojoa Acosta et al.<sup>27</sup> proposed a two-staged DL-based method for the automated localization and categorization of melanoma-affected areas. In the first step, mask and region-based CNN networks were used to automatically crop the ROI within an input sample. In the following stage, a ResNet152 classifier was used to determine whether a lesion is benign or malignant. Zhang et al.<sup>28</sup> presented a fully convolution network (FCN) based approach for the segmentation of melanoma lesions. In the FCN, the VGG16 architecture was employed as a base network to compute representative feature sets. In addition, a shallow network was utilized to integrate hand-crafted texton-based spatial features. This method<sup>28</sup> performs well as compared to existing approaches; however, the performance degrades on samples having lesions with very complex shapes and homogeneous appearances. Shan et al.<sup>29</sup> employed a framework named FC-dual-path network (FC-DPN) for improved segmentation of melanoma-affected regions. The architecture was based on FCN, in which the dense blocks were replaced by DPN blocks for robust keypoint computation. The DPN blocks are further decomposed into two sub-blocks: the DPN-projection and the DPN-processing unit, to effectively re-explore and reuse features. This method<sup>29</sup> shows an accuracy of 95.14% on the modified ISBI 2017 database, however, has considerable computational expenses.

Lei et al.<sup>30</sup> suggested an automated melanoma diagnostic technique. The method was based on the ResNet-based fully convolutional networks (ResFCN) that were separately trained for specific classes, that is, melanoma affected, non-affected, and combined images. The trained models were then used to estimate the probability of individual pixels that were integrated iteratively to generate the final segmentation map of the melanoma lesion area. This approach<sup>30</sup> achieved an overall accuracy of 95.78% on the ISBI 2016 database; however, it suffers from a higher computing overhead. Adegun et al.<sup>31</sup> introduced a pixel-wise classification approach for melanoma lesion categorization. After performing preprocessing, the input samples were fed to an encoder-decoder-based network that was followed by a softmax layer for pixel-wise classification. The identified ROI was further classified into

melanoma affected or healthy class. This approach<sup>31</sup> shows robust performance and performs real-time analysis and diagnosis; however, it suffers from overfitting issues. Nawaz et al.<sup>32</sup> developed a method for identifying and segmenting melanoma lesions in dermoscopic images. Preprocessed samples were first passed to the DL algorithm, namely, Faster-RCNN to locate the ROI, and then segmentation was performed using fuzzy k-mean clustering to segment the melanoma-affected region of skin having varying sizes and shapes. This method showed the highest accuracy of 95.6% on the PH2 database. Similarly, Nawaz et al.<sup>33</sup> used SVM to perform classification on the localized melanoma region through faster-RCNN. This technique<sup>33</sup> performs better in terms of classification due to its ability to deal with overfitting data. However, the performance of these approaches<sup>32,33</sup> depends on hyper-parameters selected during training. Banerjee et al.<sup>34</sup> presented an approach for locating and segmenting melanoma cells. The approach used a DL framework called YOLO that computes deep keypoints and determines the exact location of the melanoma region by using the bounding box in dermoscopic samples. Then, a segmentation process was carried out to determine the exact affected area of the melanoma moles by utilizing graph theory and L-type fuzzy number-based approaches. This approach<sup>34</sup> exhibits improved melanoma segmentation accuracy, however, it is unable to accurately discriminate small-sized melanoma lesions. Iqbal et al.<sup>35</sup> suggested a novel deep CNN architecture to perform multi-class categorization of melanoma lesions. The model is comprised of four key-kernel units and 68 convolution layers for discriminative feature calculation and the FC layer for classification. This approach<sup>35</sup> shows improved categorization accuracy and is computationally efficient; however, it requires the evaluation of diverse types of samples. Khan et al.<sup>36</sup> presented an object recognition-based framework for melanoma lesion identification. The approach was based on the Mask R-CNN method, which localizes and segments the melanoma lesion using the ResNet50 structure for deep keypoint computation. The lesion area was then classified using features obtained from the DenseNet201 network that was subsequently optimized using entropy-controlled least square SVM. This work<sup>36</sup> reported the highest segmentation and classification accuracy of 93.6% and 96.3%, respectively, on the ISBI2016 database; however, it is computationally costly. Some other studies also performed skin lesion classification and segmentation.<sup>37–43</sup> We have presented the critical analysis of existing approaches for the noma moles recognition in Table 1.

Although the aforementioned algorithms outperformed in identifying skin cancer from dermoscopic

images, however, their performance still has to be improved for applications in real-world and clinical situations. Furthermore, the cost of computing for these algorithms is a significant barrier in clinical applications.

### 3 | PROPOSED METHODOLOGY

In this work, a DL-based approach, namely, an improved UNET model with DenseNet-77 as backbone architecture is presented to segment the skin lesions. The presented framework includes three major phases: (i) preprocessing, (ii) network training, and (iii) melanoma moles segmentation. In the first phase, a data preprocessing approach is used to remove the undesired information from the input images and improve the visual quality of samples. Then, the DenseNet77-based UNET model is trained on the processed samples to segment the melanoma moles. We introduced the UNET model with the DenseNet-77 approach as its backbone for keypoints calculation. The DenseNet-77 approach uses deep links to recall pixel values that may be unexploited due to the usage of the pooling operations. The UNET framework comprises two modules named the encoder and decoder, respectively. In our proposed work, the encoder module uses the DenseNet77 approach to extract the reliable set of image keypoints, and the decoder module employs the UNET genuine decoder. The whole flow followed by the introduced approach is demonstrated in Figure 1.

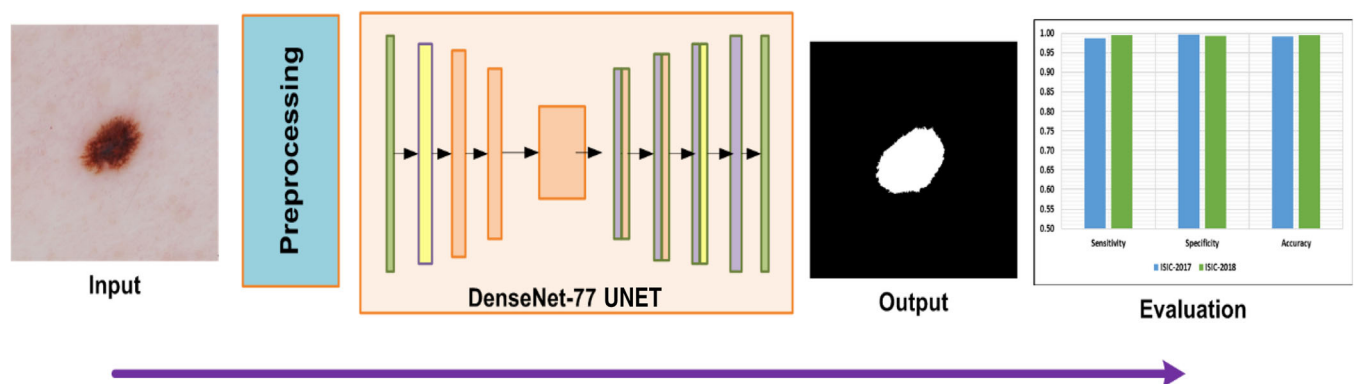
#### 3.1 | Preprocessing

In the field of medicine, extensive work is presented to employ the images to segment the diseased portion like melanoma lesions. However, it is quite difficult to capture the samples of affected areas without the brightness and chrominance changes in them. Such artifacts usually occurred in images because of the quick alterations in the lightning source, or the light reflected by the skin regions.

The occurrence of such artifacts in the input samples can reduce the identification and segmentation results of the employed model. Moreover, in the melanoma-affected samples, the existence of hair and tiny blood vessels also complicates the diseased region segmentation power. To cope with such challenges, we have performed a preprocessing step on the suspected images via employing the morphological closing method to eliminate the unnecessary artifacts. Furthermore, an un-sharp filter<sup>45</sup> is used to enhance the visual appearance of the input images which assists in better locating the skin

**TABLE 1** Comparative analysis of existing methods for skin cancer recognition

References	Year	Method	Task	Dataset	Accuracy
<i>Hand-crafted methods</i>					
20	2017	The gray level co-occurrence matrix along with the support vector machine (SVM) classifier	Classification	Custom dataset	92.1%
22	2017	The UNET model + deep features along with the SVM classifier	Classification	ISIC-2016	76%
23	2020	A hybrid model comprising scale-invariant feature transform (SIFT) feature extractor along with the SVM and KNN classifier	Classification	ISIC-2017	88.40%
24	2021	The Gaussian Mixture Model framework with the region growing based approach for segmentation	Segmentation	PH2	86.83%
25	2019	The SIFT descriptor along with the SVM classifier	Classification	PH2	82%
42	2021	LVP + LBP along with C means clustering	Segmentation	PH2	79.44%
<i>DL-based approaches</i>					
26	2020	AlexNet	Classification	HAM10000	84%
27	2021	ResNet152	Classification	ISIC-2017	90.40%
28	2019	VGG16	Classification	ISIC-2017	92.72%
29	2020	FC-DPN	Segmentation	ISIC-2017	95.14%
30	2019	ResFCN	Segmentation	ISIC-2016	95.78%
31	2019	Encoder-decoder-based network	Classification	ISIC-2017	95%
32	2021	Faster-RCNN along with the FKM	Segmentation	PH2	95.6%
33	2021	Faster-RCNN with the SVM classifier	Classification	ISIC-2016	89.10%
34	2020	YOLO along with the L-type fuzzy clustering	Segmentation	ISIC-2017	97.33%
35	2021	Convolutional neural network	Classification	ISIC-2019	88.75%
36	2021	Mask-RCNN, DenseNet201 along with the SVM classifier	Segmentation	ISIC-2016	93.6%
37	2022	Fully Convolution Encoder-Decoder Network	Segmentation	ISIC-2016	98.32%
38	2021	Bayesian deep learning method	Classification	Kaggle Skin Cancer dataset	88.95%
39	2021	Metadata processing block-based method	Classification	ISIC-2019	74.90%
40	2022	U-Net	Segmentation	ISIC-2017	94.67%
41	2022	U-Net++	Segmentation	ISIC-2018	95.30%
44	2021	DCNN	Classification	HAM10000	91.93%

**FIGURE 1** Proposed method flow diagram



cancer moles from the input images. Equation (1) is presenting the mathematical description of the morphological closing operator.

$$I_x(i,j) = (I(i,j) \oplus E) \ominus E. \quad (1)$$

Here,  $I(i,j)$  exhibits the input sample,  $i$  and  $j$  are presenting the position of the pixels, while,  $E$  is showing the structuring window having a size of 10 in squared shape and the angle of  $90^\circ$  and  $180^\circ$  for all pixel values. The  $I_x(i,j)$  is showing the enhanced sample by eliminating the presence of hair or tiny blood vessels. Though the applied approach assists to remove the unrequired artifacts from the input images, it also generates the effect of blurriness in the processed images. Therefore, an unsharp filter is applied to minimize the impact of blurring and enhance the visual quality of samples. Equation (2) is showing the description of the used unsharp filter:

$$I_p(i,j) = I_x(i,j) \times \varpi(i,j). \quad (2)$$

$$\varpi(i,j) = -\frac{1}{\pi\sigma^4} \left[ 1 - \frac{i^2 + j^2}{2\sigma^2} \right] e^{-\frac{i^2 + j^2}{2\sigma^2}}. \quad (3)$$

The results sample  $I_o(i,j)$  is acquired by utilizing Equation (4) that only contains the required information necessary for melanoma moles segmentation.

$$I_o(i,j) = I(i,j) - I_p(i,j). \quad (4)$$

### 3.2 | UNET model

A reliable group of sample keypoints is necessary to perfectly segment the melanoma lesions from the input images. While the mentioned reasons hinder the procedure of extracting a representative set of keypoints from the samples: (i) the usage of large-sized keypoints results in the model over-fitting issue, and (ii) the usage of less number of a feature set can obstruct the network to acquire the significant characteristic of the lesion structure, that is, the size, color, shape, and orientations of melanoma moles. To avoid the occurrence of such issues, it is mandatory to introduce a fully automated keypoints computation approach without the need of using the hand-coded feature extraction approaches. The methods employing hand-coded keypoints calculation methods are not robust to segment the melanoma-affected regions due to the extensive changes in the size, shape, and architecture of moles. Consequently, to deal with the aforesaid issues, a DL-based approach named improved UNET

model along with the DenseNet-7 framework as backbone architecture is presented to learn a more robust set of deep features from the input images. The convolution filters of UNET calculate the features of the suspected samples by observing their structure.

Even though, the research community has presented numerous conventional segmentation methods like edge detection,<sup>46,47</sup> region-based,<sup>48,49</sup> and pixel-based methods.<sup>50</sup> However, the main reason to nominate the UNET approach in comparison to the above-mentioned approaches is that these methods are unable to tackle the advanced complexities of sample segmentation, that is, the huge alterations in the shape, shade, and mass of melanoma lesions. Additionally, such methods are economically expensive and are unable to be deployed for the real-world scenarios due to their extensive processing requirements. While in comparison, the UNET approach is more robust both in terms of the model architecture and lesion segmentation. Furthermore, it needs small data to perform the network training which makes it computationally efficient in comparison to other segmentation approaches.

### 3.3 | Custom-UNET

The UNET model contains two main units which are as follows: (i) encoder and (ii) decoder. The main work of the first part, namely, the encoder is to extract the representative set of features from the input images. Whereas, the second unit is the symmetric growing track employed to achieve the precise localization of suspected objects by utilizing the transferred convolutions. The conventional UNET encoder contains the redundant application of  $3 \times 3$  convolutions, in which all layers have the ReLU activation method together with the  $2 \times 2$  max-pooling layers containing the stride degree of 2 to execute the down-sampling. The down-sampling phase doubled the feature channels. Whereas the decoder unit executes the up-sampling process, where the keypoints map parallels to a  $2 \times 2$  up-convolution layer halves the keypoints channels and implements concatenation with the cropped feature map from the encoder part. The traditional UNET model uses skip links to omit non-linear transformations which causes to loss of the important pixel information and results in the vanishing gradient issue. To deal with the problems of the traditional UNET framework, an improved UNET model is presented by introducing a deeply connected CNN framework, namely, DenseNet77 to replace the encoder unit of the original framework. The DenseNet-77 encoder-based UNET model is shown in Figure 2.

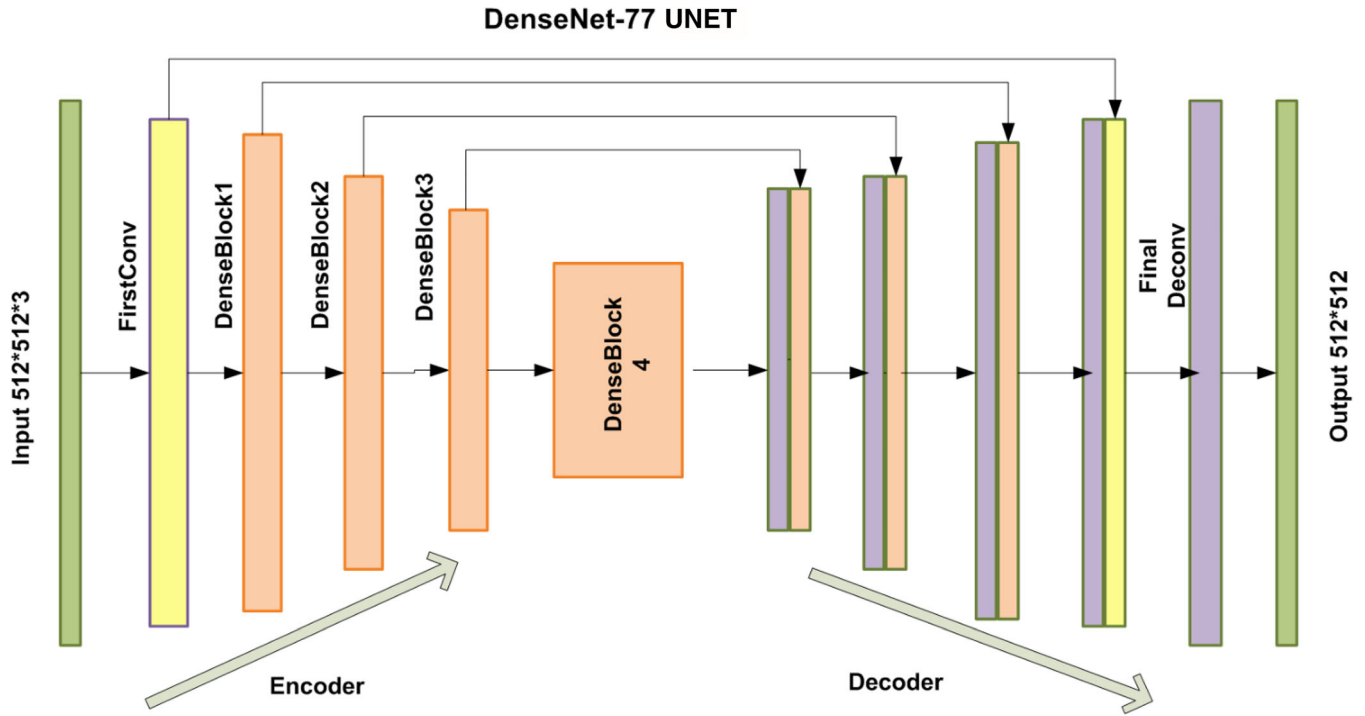


FIGURE 2 DenseUNet architecture

The introduced DenseNet-77 keypoints computer has fewer model parameters in comparison to the original encoder of the UNET approach. The DenseNet approach has many dense blocks (DnBs) that are sequentially inter-linked by proposing added convolutional layers ( $Cn_L$ ) along with the pooling layers ( $Po_L$ ) in succeeding DnBs.<sup>51,52</sup> The DenseNet method is more powerful to exploit the complicated sample transformations which assist to tackle the issue of absent object position information to efficiently identify it. Also, the DenseNet model supports the features diffusion procedure and improves their reemployment which permits it to be used for skin lesion detection and segmentation. Therefore, in the presented method, we have used the DenseNet-77 encoder-based UNET approach for extracting the reliable set of image features.

### 3.4 | DenseNet-77-based UNET encoder

The encoder unit uses a CNN framework to calculate the keypoints from the input samples. After keypoints computation, it performs the down-sampling step to reduce the feature size and attain the detailed image information. The conventional encoder of the UNET model produces sample keypoints maps by eliminating the resolution of the original images. So, to resolve this problem we have used the DenseNet-77 framework as a base network in the encoder unit which is a more reliable network with adequate depth, size, and resolution.

TABLE 2 Architectural description of DenseNet-77

Densenet-77		
Layer	Dimension	Stride
$Cn_L$ 1	$7 \times 7$ cn	2
$Po_L$ 1	$3 \times 3$ max_pool	2
Dense block (DnB) 1	$\begin{bmatrix} 1 \times 1 \text{ cn} \\ 3 \times 3 \text{ cn} \end{bmatrix} \times 6$	1
$Tn_L$ $Cn_L$ 2	$1 \times 1$ cn	1
$Po_L$ 2	$2 \times 2$ average_pool	2
DnB 2	$\begin{bmatrix} 1 \times 1 \text{ cn} \\ 3 \times 3 \text{ cn} \end{bmatrix} \times 12$	1
$Tn_L$ $Cn_L$ 3	$1 \times 1$ conv	1
$Po_L$ 3	$2 \times 2$ average_pool	2
DnB 3	$\begin{bmatrix} 1 \times 1 \text{ cn} \\ 3 \times 3 \text{ cn} \end{bmatrix} \times 12$	1
$Tn_L$ $Cn_L$ 4	$1 \times 1$ cn	1
$Po_L$ 4	$2 \times 2$ average_pool	2
DnB 4	$\begin{bmatrix} 1 \times 1 \text{ cn} \\ 3 \times 3 \text{ cn} \end{bmatrix} \times 6$	1
Classification layer	$7 \times 7$ average_pool	
	Fully connected	
	SoftMax	

Furthermore, the DenseNet-77 approach is computationally better than that of the conventional UNET encoder because of its small number of model parameters.

The employed Densenet-77 approach has two main distinctions from the traditional DenseNet model which are listed as follows: (i) Densenet-77 contains minimum model parameters as the conventional DenseNet has 64 keypoints channels. Whereas in comparison the Densenet-77 has only 32 keypoints channels, with the filter dimension of  $3 \times 3$  in the place of a  $7 \times 7$  filter size (ii) Furthermore, all layers of the DnBs are attuned to reduce the computational burden. The detailed architectural information of the DenseNet-77 is described in Table 2 which shows the layer's name used for keypoints

calculation to execute the enhanced processing by the improved-UNET model. Furthermore, the graphic explanation of the DenseNet-77 given in Figure 3 was for all layers,  $s \times s \times t_0$  is showing the features maps (FMs) with  $s$  and  $t_0$  exhibiting the FMs dimension and total channels, respectively. Moreover, the  $f(\cdot)$  is showing a non-linear transformation method with numerous functions, namely, Batch Normalization (BaNr), ReLU, and a  $1 \times 1$  Cn<sub>L</sub> to minimize the channel information. Besides, a  $3 \times 3$  Cn<sub>L</sub> is used to implement the keypoints reformation. The dense links found among the successive layers

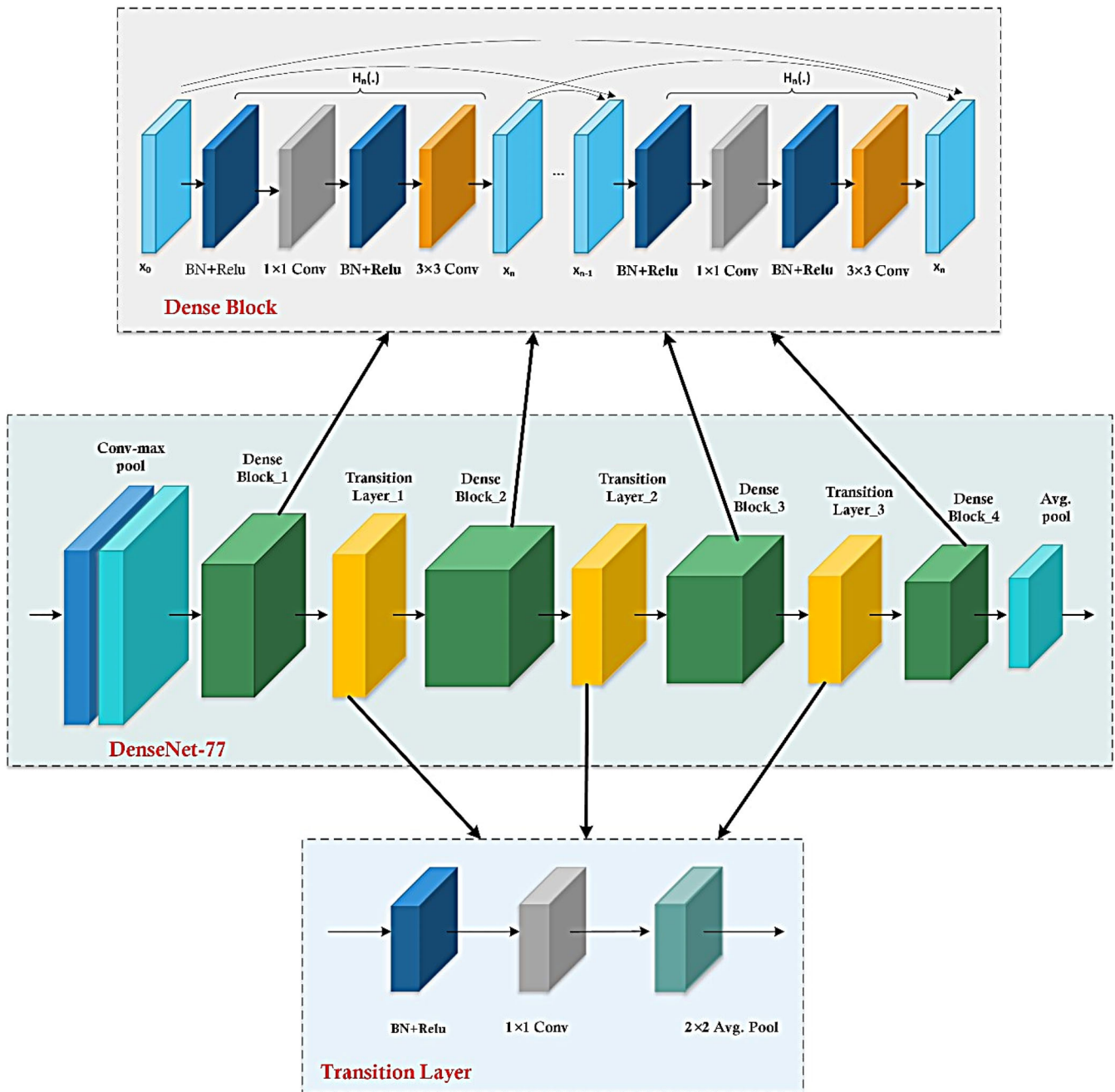


FIGURE 3 Comprehensive structural demonstration of DenseNet-77 together with the dense blocks and TnL architecture



are demonstrated by the long-dashed sign and the  $s \times s \times (t_0 + 2t)$  is the outcome of the last layer. The dense links of the DenseNet-77 increase the FMs which are minimized by introducing the transition layer ( $Tn_L$ ) at the end of all DnBs.

### 3.5 | UNET decoder

The decoder is the second unit of the UNET framework containing several  $Cn_{LS}$ ,  $Pol_S$ , and activation layers to acquire the accurate localization of the region of interest (RoIs). The decoder unit uses the output from the encoder phase to further explore them by passing the values to the expansion path. The decoder unit works by combining the feature maps obtained from the encoder unit containing the data about both the high-level keypoints and their corresponding pixel information. The obtained data from the encoder is passed to several up-convolutions to perform the concatenation. In our work, the UNET encoder uses the DenseNet-77 framework as the backbone network, while the decoder unit is the same as the conventional UNET model employed.

### 3.6 | Detection process

Once the model training is completed, the test samples are employed to evaluate them over the trained model. A method is utilized to visually show the prediction made by the trained model for skin moles segmentation. The method requires the input, and output array, together with model predictions. The prediction unit provides the result by showing the image together with the estimated mask related to a particular sample.

## 4 | RESULTS AND DISCUSSION

In this section, we have discussed the details of datasets and metrics used to check the segmentation performance of the proposed approach. Moreover, we have performed several experiments to evaluate the approach in numerous ways to show the robustness of the presented technique.

### 4.1 | Datasets

We have used two datasets, namely, ISIC-2017 and ISIC-2018 to validate the melanoma lesion segmentation power of the proposed approach. Both datasets are

TABLE 3 Detailed description of employed datasets

Dataset	Total samples	Training images	Validation images	Test images
ISIC-2017	2750	2000	150	600
ISIC-2018	3694	2594	100	1000

published by the “International Symposium on biomedical images (ISBI) in the challenge of Skin lesion analysis towards Melanoma detection”.<sup>53</sup> The description of both datasets is given in Table 3. Therefore, we have used the training dataset by dividing it into 70% and 30% for both the model training and testing, respectively. All the ground truths available in both databases are evaluated by a board of dermatologists. The purpose of choosing the ISIC databases for the proposed model assessment is that these contain images that are complex in nature and are suffering from several image distortions like holding the variations in the size, position, and color of lesions. Moreover, the mole images contain hair and tiny blood vessels which complicates the lesion segmentation process. Additionally, samples have light variations and contain noise and blurring. All the aforementioned reasons have made the ISIC datasets more complicated and closer to real-world scenarios.

The proposed approach is trained for 20 epochs and the training curve along with the loss graph is presented in Figure 4 that clearly shows that the model did not overfit during its training.

### 4.2 | Evaluation metrics

For model evaluation, we have selected several standard metrics, namely, sensitivity, specificity, accuracy, dice coefficient, and Jaccard index to check the melanoma moles segmentation power of our work. The mathematical explanation of employed metrics is demonstrated from Equations (5) to (8):

$$\text{Specificity} = \frac{TP}{TP + FP}. \quad (5)$$

$$\text{Sensitivity} = \frac{TP}{TP + FN}. \quad (6)$$

$$\text{Accuracy} = \frac{TP + TN}{TP + FP + TN + FN}. \quad (7)$$

$$\text{Dice} = \frac{2 \times TP}{2 \times TP + FN + FP}. \quad (8)$$

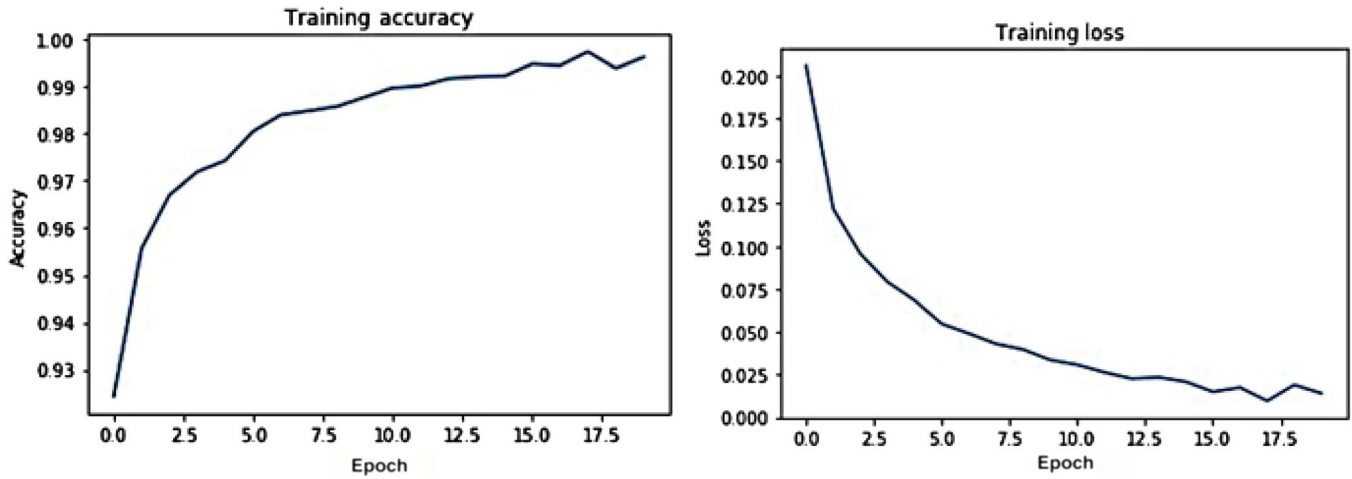


FIGURE 4 Visual demonstration of training accuracy graph and training loss graph curves, respectively

### 4.3 | Evaluation of proposed method

An accurate melanoma segmentation model should be capable of precisely segmenting the lesions of varying sizes and shapes. For this reason, we have designed an experiment to validate the proposed approach. To accomplish this task, we have taken the samples from both datasets, namely, the ISIC-2017 and ISIC-2018 and tested them via the trained model. The images are selected with the changes in the size, shape, color, and position of lesions to better demonstrate the recognition ability of the improved UNET model. The preprocessing results are presented in Figure 5. The visual result of the proposed approach for the ISIC-2017 and ISIC-2018 datasets are shown in Figure 6. It can be seen from the reported results that our model has correctly segmented the melanoma moles and is robust to alterations found in the structure of skin lesions.

We further elaborate the segmentation power of our model by numerically reporting the segmentation results. We have considered several standard evaluation metrics and the results for both used datasets are shown in Table 4. More specifically, for the ISIC-2017 dataset, we have attained the average sensitivity, specificity, and accuracy values of 98.73%, 99.66%, and 99.21%, respectively. Similarly, for the ISIC-2018 dataset, we have acquired the average sensitivity, specificity, and accuracy values of 99.44%, 99.35%, and 99.51%, respectively. Moreover, we have presented the Jaccard index and dice coefficient for both datasets via using the boxplot (Figure 7). For the ISIC-2017 dataset, we have attained the Jaccard index and dice score of 0.9688 and 0.9802 which is 0.9771 and 0.9873 for the other dataset. Furthermore, the confusion matrixes for both datasets are reported in Figure 8.

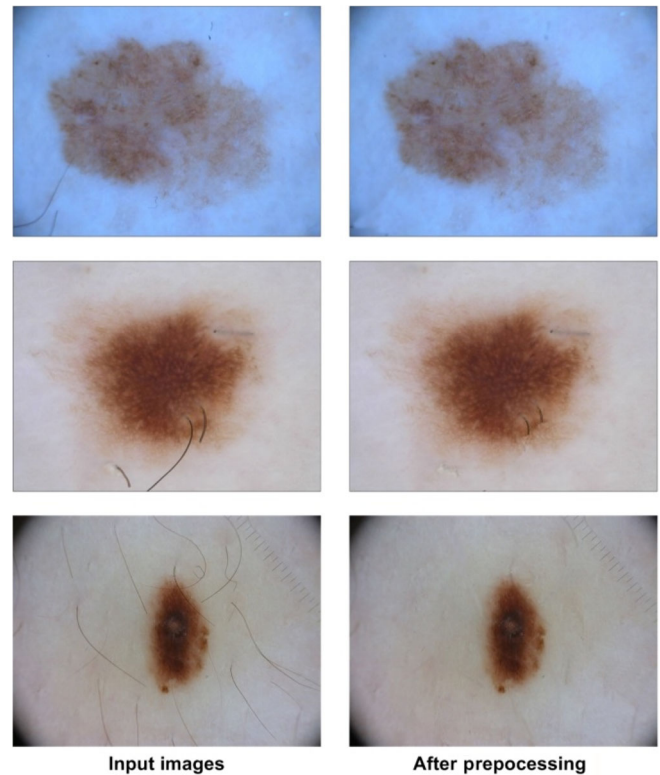


FIGURE 5 Preprocessing results

Both the visual and numeric results are clearly showing that our approach has accurately segmented the melanoma lesions with a high recall rate and better accuracy value. The main reason for the robust performance of our approach is due to the robust feature selection power of the DenseNet-77 network which shows the complicated image transformations in a more suitable way which ultimately enhances the recognition power of the proposed approach.

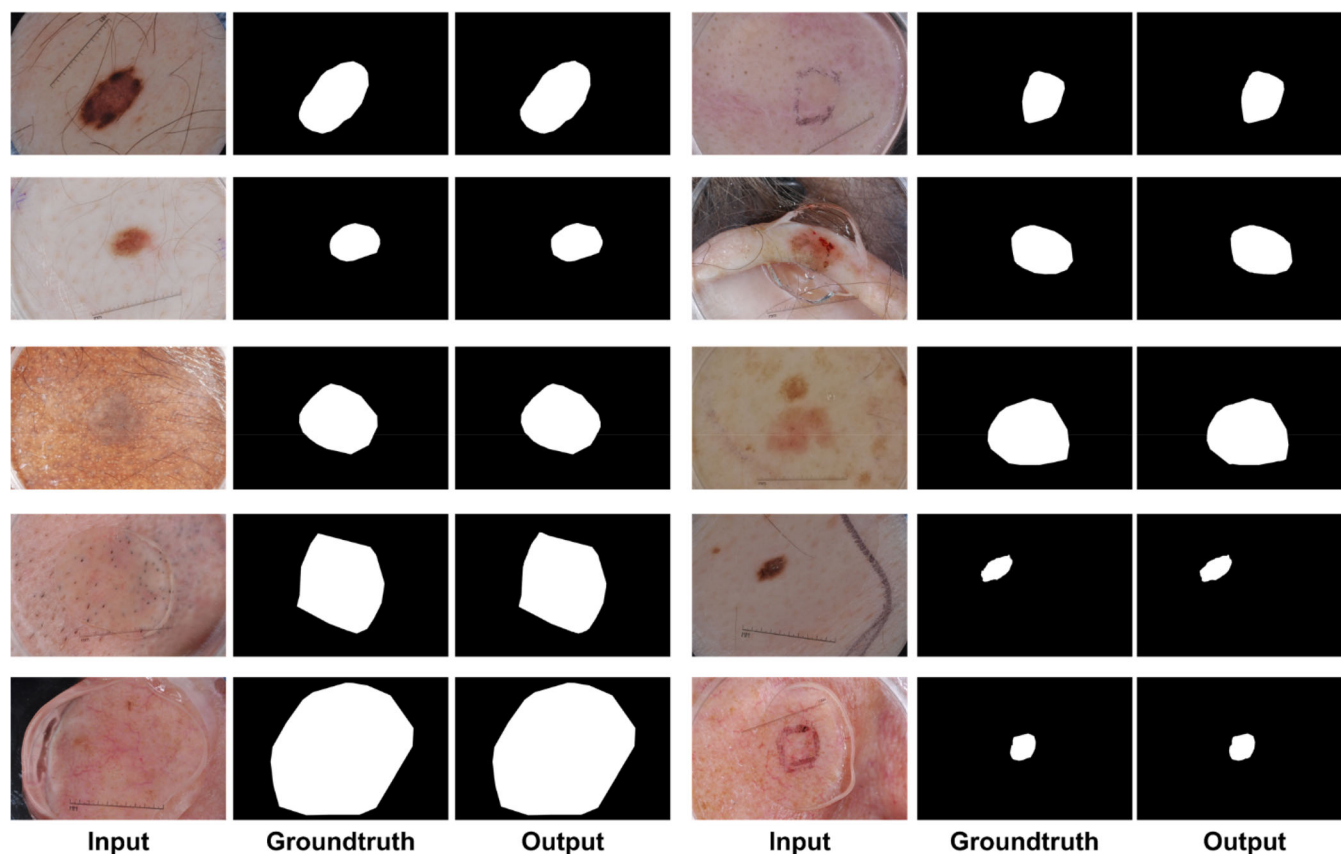


FIGURE 6 Proposed method segmentation results

TABLE 4 Performance of our method on two datasets

Dataset	Sensitivity	Specificity	Accuracy
ISIC-2017	98.73%	99.66%	99.21%
ISIC-2018	99.44%	99.35%	99.51%

#### 4.4 | Comparison with challenge teams

Here, we have presented the comparison of the proposed approach with the results reported on the competition leaderboard. The results for both ISIC-2017 and ISIC-2018 databases are described in Tables 5 and 6, respectively, and sorted based on the Jaccard index metric. Table 5 presents the segmentation results of the Top 5 teams obtained over the test samples using the ISIC-2017 database. The results mentioned in Table 5 are taken from the ISIC2017 competition leaderboard. Based on the results presented in Table 5, we can observe that our approach outperformed the other competitors in terms of overall performance. The methods mentioned in References 54–58 obtained an accuracy of 93.4%, 93.2%, 93.4%, 93.1%, and 93.0%, whereas the proposed approach attained an accuracy of 99.21%. More specifically, our proposed algorithm showed an improvement in the JSI

score with a value of 96.88% in comparison to the top-placed methods<sup>54–58</sup> and an overall gain of 21.02%. A similar trend is observed for all other metrics.

We have also presented the segmentation results of the Top 3 teams of the ISBI2018 database in Table 6. It is noted that the methods are not directly citable and the results mentioned here are taken from Reference 59. From Table 6, it can be seen clearly that our method shows superior performance in terms of all major evaluation metrics such as the Jaccard index, dice, and accuracy. The proposed method obtained the 99.51% accuracy, 98.73% dice score, 97.71% Jaccard index, 99.44% sensitivity, and 99.35% specificity that is 5.17%, 8.66%, 14.07%, 7.51%, and 3.38% improved in comparison to the first-placed technique on the ISIC-2018 challenge. According to the given comparison, these findings show that the suggested algorithm is capable of achieving good segmentation outcomes in comparison to top-ranked techniques on the same databases.

#### 4.5 | Comparison with base models

In this section, we have compared the segmentation power of our approach against several base models. To

accomplish this, we have taken the results of the UNET model with other base approaches like VGG16,<sup>60</sup> ResNet50,<sup>61</sup> MobileNetV3,<sup>62</sup> DenseNet201,<sup>63</sup> and

EfficientNet<sup>64</sup> to compare the obtained performance against them. To have a fair comparison, we have considered both the evaluation results and architectural

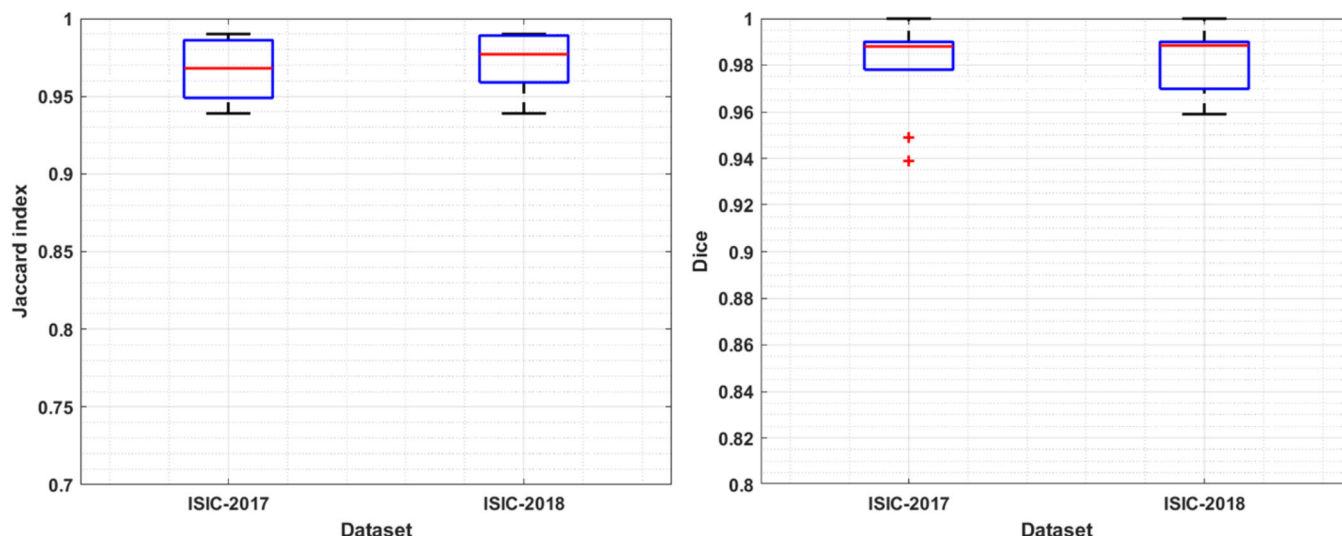


FIGURE 7 Proposed system performance in terms of Jaccard index and dice score

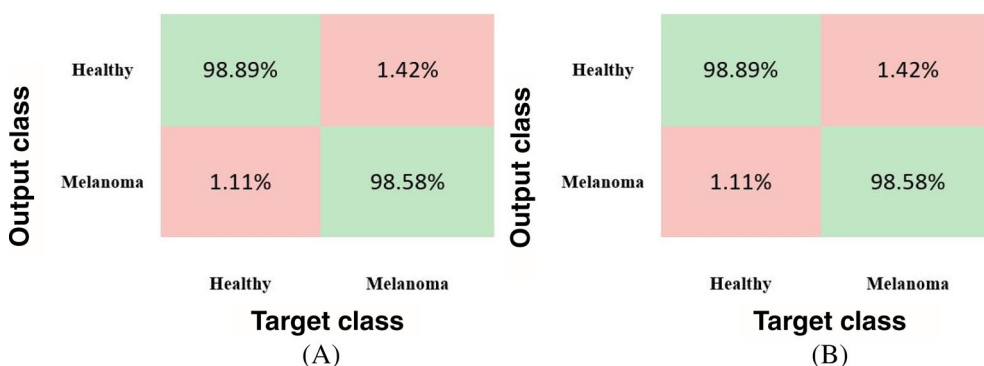


FIGURE 8 Confusion matrixes for the ISIC-2017 dataset as (A) and the ISIC-2018 dataset as (B)

TABLE 5 Segmentation results from ISIC-2017 competition leaderboard

Method	Jaccard index (%)	Dice (%)	Accuracy (%)	Specificity (%)	Sensitivity (%)
CDNN <sup>54</sup>	76.5	84.9	93.4	97.5	82.5
U-Net <sup>55</sup>	76.2	84.7	93.2	97.8	82.0
Deep residual network <sup>56</sup>	76.0	84.4	93.4	98.5	80.2
U-Net <sup>57</sup>	75.4	83.9	93.1	96.9	81.7
FCNN <sup>58</sup>	75.2	83.7	93.0	97.6	81.3
Proposed	96.88	98.02	99.21	99.66	98.73

TABLE 6 Segmentation results from ISIC-2018 competition leaderboard

Method	Jaccard index (%)	Dice (%)	Accuracy (%)	Specificity (%)	Sensitivity (%)
MaskRcnn2 + segmentation	83.8	89.8	94.2	96.3	90.6
Ensemble with CRFv3	83.7	90.4	94.5	95.2	93.4
Lesion segmentation by DCNN	83.4	90.0	94.3	96.4	91.8
Proposed	97.71	98.73	99.51	99.35	99.44



complexity by considering the model parameters as well. For both databases, namely, the ISIC-2017 and ISIC-2018, the obtained evaluation results are shown in Table 7.

It is quite evident from the results shown in Table 7 that our work is more robust to melanoma segmentation as compared to other base approaches for both datasets. For the ISIC-2017 dataset, the lowest results are exhibited by the VGG16-based UNET model with an accuracy of 92.48%. The second-lowest segmentation performance is shown by the ResNet50-based UNET model. While for the ISIC-2018 dataset, the lowest results are acquired by the ResNet50-based UNET with an average segmentation accuracy of 88.50%. Whereas, in the case of model complexity, the DenseNet201-based UNET approach is the most expensive with the 41.80 million model parameters. While in the comparison, the proposed UNET approach provides a better tradeoff between the segmentation performance and model parameters with the average segmentation accuracy values of 99.21%, and 99.51% for the ISIC-2017 and ISIC-2018 datasets, respectively. The results depicted in Table 7 are clearly demonstrating that the proposed framework shows the highest results for all reported evaluation parameters and minimizes the computational burden as well. The introduced DenseNet-77 at the encoder section of the UNET model has not only assisted the framework to compute a more representative set of image features but also helps to reduce the computational burden as well. Hence, we can conclude that our approach is more efficient and effective for skin moles segmentation.

#### 4.6 | Comparison with state-of-the-art

To further explain the segmentation power of our model, we have taken several latest approaches from history and compared our results against them. To have a fair comparison, we have taken the average results of our approach and compared them with the average results of all selected studies.

First, to compare the segmentation results obtained on the ISIC-2017 dataset, we have considered the work mentioned in References 65–72 and obtained results are described in Table 8. Gu et al.<sup>65</sup> proposed a DL-based approach, namely, a deep edge convolutional neural network (DE-Net) for the automated segmentation of skin moles. Initially, a ResNet50-based encoder was used for deep feature computation which was later segmented by the decoder of the DE-Net. The work attained an average segmentation accuracy of 94.50% along with the Jaccard index and dice coefficient of 0.8053 and 0.8792, respectively. Another DL-based approach was presented in

TABLE 7 Comparison with base models

Model	Sensitivity (%)			Specificity (%)			Accuracy (%)			Dice coefficient			Jaccard index			Parameters (million)	Time (s)
	ISIC-2017	ISIC-2018	ISIC-2018	ISIC-2017	ISIC-2018	ISIC-2018	ISIC-2017	ISIC-2018	ISIC-2018	ISIC-2017	ISIC-2018	ISIC-2018	ISIC-2017	ISIC-2018	ISIC-2018		
VGG16-UNET	78.64	70.80	96.40	97.16	97.16	96.40	92.48	89	89	0.8409	0.647	0.647	0.7595	0.549	0.549	23.8	0.0277
ResNet50-UNET	82	85.90	92.70	97	97	92.70	93.04	88.50	88.50	0.8608	84.40	84.40	0.7816	78.12	78.12	32.6	0.0230
MobileNetV3-UNET	86.24	90.89	96.38	96.36	96.36	96.38	93.81	94.79	94.79	0.8774	0.9098	0.9098	0.8025	0.8344	0.8344	8.27	0.0199
DenseNet201-UNET	87.73	89.60	94.38	-	-	94.38	94.55	91.67	91.67	-	88.50	88.50	0.8110	81.49	81.49	41.80	0.0261
EfficientNet-UNET	-	-	-	-	-	-	-	-	-	0.861	0.912	0.912	0.781	0.846	0.846	-	-
Proposed	98.73	99.44	99.35	99.66	99.66	99.35	99.21	99.51	99.51	0.9802	0.9873	0.9873	0.9688	0.9771	0.9771	6.2	0.0178



Reference 66 for skin lesion segmentation from the dermoscopic images and acquired the average segmentation accuracy value of 93.26% along with the Jaccard index and dice score of 0.7653 and 0.8500, respectively. Khoulood et al.<sup>68</sup> presented a DL-based approach, namely, W-net to identify and segment the melanoma moles with an average segmentation accuracy of 97.94%. Banerjee et al.<sup>67</sup> proposed a deep CNN approach for skin lesion segmentation and attained an average segmentation accuracy of 98.67%. Moreover, the approach in Reference 69 shows a sensitivity value of 86%, while the techniques<sup>70–72</sup> attain the accuracy values of 94.08%, 94.30%, and 93.13%, respectively. Whereas, it can be seen from Table 8 that our work outperforms the comparative approaches in terms of all employed metrics. More specifically, in terms of the sensitivity metric, the comparative approaches show an average value of 88.90%, which is 98.73% for our case. Hence, for the sensitivity metric, the proposed approach gives an average performance gain of 9.83%. Similarly, for the specificity and accuracy metrics, the selected methods show the average values of 98.06% and 95.13%. Whereas, the presented technique shows the average specificity and accuracy values of 98.06% and 99.21%. Therefore, for the specificity and accuracy the improved UNET approach gives the average performance

gains of 1.6% and 4.08%, respectively. Similarly, for the Jaccard index and dice coefficient, the competitor approaches show the average values of 0.8129 and 0.8937, respectively, which are 0.9688 and 0.9802 for our method. Therefore, for the Jaccard index and dice coefficient metrics, we have presented the average performance gains of 15.59% and 8.65%, respectively.

Similarly, for the ISIC-2018 dataset, we have selected the works elaborated in References 66–70,73–75 and comparative results are shown in Table 9. Wu et al.<sup>66</sup> proposed an approach, namely, FAT-Net to detect and segment the skin lesions and attained an average segmentation accuracy of 95.78%. Another DL-based approach was presented in Reference 68 to segment the skin moles and showed an average accuracy of 97.39%. Similarly, in Reference 67 a deep CNN method was proposed to automatically segment the skin moles with an average segmentation accuracy of 98.96%. Araújo et al.<sup>73</sup> introduced an automated framework, namely, the LinkNet to identify and segment the skin moles with an average segmentation accuracy of 96.70%. Moreover, the methods in References 69,75 show the sensitivity values of 86% and 78.90%, respectively, while the approaches in References 70,74 attain the accuracy values of 97.20% and 96.19%, respectively. From the results reported in

Study	Sensitivity	Specificity	Accuracy	Jaccard index	Dice
Gu et al. <sup>65</sup>	88.04%	96.59%	94.50%	0.8053	0.8792
Wu et al. <sup>66</sup>	83.92%	97.25%	93.26%	0.7653	0.8500
Khoulood et al. <sup>68</sup>	94.86%	98.89%	97.94%	-	0.9322
Banerjee et al. <sup>67</sup>	96.95%	99.50%	98.67%	0.9598	0.9795
Hasan et al. <sup>69</sup>	86%	-	-	-	-
Dai et al. <sup>70</sup>	-	-	94.08%	0.7855	0.8648
Kaur et al. <sup>71</sup>	-	-	94.30%	-	-
Ramadan et al. <sup>72</sup>	83.64%	-	93.13%	0.7488	0.8563
Proposed	98.73%	99.66%	99.21%	0.9688	0.9802

**TABLE 8** Comparison with state-of-the-art methods over ISIC-2017 dataset

Study	Sensitivity	Specificity	Accuracy	Jaccard index	Dice
Wu et al. <sup>66</sup>	91.00%	96.99%	95.78%	0.8202	0.8900
Khoulood et al. <sup>68</sup>	95.54%	98.40%	97.39%	-	0.9300
Banerjee et al. <sup>67</sup>	99.10%	98.78%	98.86%	0.9566	0.9778
Araújo et al. <sup>73</sup>	86.20%	98.60%	96.70%	0.8000	0.8890
Hasan et al. <sup>69</sup>	86%	-	-	-	-
Santos et al. <sup>74</sup>	86.91%	98.09%	97.20%	0.9757	-
Dai et al. <sup>70</sup>	90.49%	-	96.19%	0.8345	0.8999
Badshah et al. <sup>75</sup>	78.90%	98%	-	0.940	-
Proposed	99.44%	99.35%	99.51%	0.9771	0.9873

**TABLE 9** Comparison with state-of-the-art methods over ISIC-2018 dataset

Table 9, it is quite evident that the proposed improved UNET approach is more robust to melanoma lesion segmentation and shows the highest results for all evaluation metrics as compared to other methods. More clearly, for the sensitivity and specificity metrics, the comparative approaches attain the average values of 89.27% and 98.14%, respectively, which are 99.44% and 99.35% for our approach. So, for the sensitivity and specificity metrics, the improved UNET approach gives the 10.17% and 1.21% of performance gains. Moreover, for the accuracy metric, the peer approaches attain the average value of 97.02%, while in comparison the presented method shows an average accuracy value of 99.51%. Hence, for the accuracy metric, the proposed approach gives an average performance gain of 2.49%. Similarly, for the Jaccard index and dice coefficient, the comparative methods show the average values of 0.8878 and 0.9173, respectively, which are 0.9771 and 0.9873 for our approach. Therefore, for the Jaccard index and dice coefficient, we have shown the average performance gains of 9.93% and 7%, respectively.

The results reported in Tables 8 and 9 confirm that our work has outperformed the existing approaches for both datasets. The main reason for the efficient performance of our approach is due to its simple network architecture that effectively reutilizes the framework parameters without using redundant feature maps. Such representation of the DenseNet-77 model causes to minimize the UNET model complexity and parameters. While in comparison, the competitor's approaches use very deep networks which eventually suffer from the model overfitting problems. The peer methods are computationally more expensive and not efficient in dealing with the several image distortions which degrade their segmentation performance. Hence, it can be said that the DenseNet-77-based UNET approach better deals with the issues of existing approaches by presenting a lightweight and more robust framework for melanoma segmentation.

## 5 | CONCLUSIONS

Melanoma at the advanced stage can cause painful treatment procedures and even can result in the death of patients. In this work, we have presented a DL-based approach for the timely and accurate detection and segmentation of melanoma lesions. A custom UNET approach with a DenseNet77-based encoder is proposed for melanoma lesion segmentation. The proposed solution is robust to locate the skin moles even under the occurrence of intense color, size, and position variations of melanoma moles. Moreover, the improved UNET model can efficiently segment the melanoma lesions under the occurrence of noise and blurring in samples.

The presented approach attains the average accuracy values of 99.21% and 99.51% over the ISIC-2017 and ISIC-2018 datasets. The reported results confirm that our proposed model can assist the practitioner in timely detecting the skin moles. The proposed approach is currently not efficient to diagnose melanoma moles under intense intensity variations. In the future, we plan to overcome this challenge by considering other DL-based approaches as the base network of the UNET model. Moreover, we plan to evaluate the introduced framework for other types of skin cancers and other medical diseases like eye abnormalities as well.

## AUTHOR CONTRIBUTIONS

All authors contributed equally to this work. All authors have read and agreed to the published version of the manuscript. Authors are thankful to Computer Lab of UET and HITEc University.

## CONFLICT OF INTEREST

The authors declare no conflicts of interest.

## DATA AVAILABILITY STATEMENT

The data that support the findings of this study are openly available in ISIC Dataset at <https://challenge.isic-archive.com/landing/2017/?msclid=a218ef74b43d11ec8a1769d50632f078>.

## ORCID

Momina Masood  <https://orcid.org/0000-0003-1977-1481>

Muhammad Attique Khan  <https://orcid.org/0000-0002-6347-4890>

Robertas Damaševičius  <https://orcid.org/0000-0001-9990-1084>

## REFERENCES

1. Siegel RL, Miller KD, Fedewa SA, et al. Colorectal cancer statistics, 2017. *CA Cancer J Clin*. 2017;67(3):177-193.
2. Rogers HW, Weinstock MA, Feldman SR, Coldiron BM. Incidence estimate of nonmelanoma skin cancer (keratinocyte carcinomas) in the US population, 2012. *JAMA Dermatol*. 2015; 151(10):1081-1086.
3. Ballerini L, Fisher RB, Aldridge B, Rees J. A color and texture based hierarchical K-NN approach to the classification of non-melanoma skin lesions. *Color medical image analysis*. Springer; 2013:63-86.
4. Cheng Y, Swamisai R, Umbaugh SE, et al. Skin lesion classification using relative color features. *Skin Res Technol*. 2008; 14(1):53-64.
5. MASOOD M, NAZIR T, NAWAZ M, JAVED A, IQBAL M, MEHMOOD A. Brain tumor localization and segmentation using mask RCNN. *Front Comput Sci*. 2020;15:156338.
6. Nazir T, Nawaz M, Rashid J, et al. Detection of diabetic eye disease from retinal images using a deep learning based CenterNet model. *Sensors*. 2021;21(16):5283.

7. Pellini B, Chaudhuri AA. Circulating tumor DNA minimal residual disease detection of non-small-cell lung cancer treated with curative intent. *J Clin Oncol*. 2022;40(6):567-575.
8. Reis HC, Turk V, Khoshelham K, Kaya S. InSiNet: a deep convolutional approach to skin cancer detection and segmentation. *Med Biol Eng Comput*. 2022;60:1-20.
9. Abdar M, Pourpanah F, Hussain S, et al. A review of uncertainty quantification in deep learning: techniques, applications and challenges. *Inf Fusion*. 2021;76:243-297.
10. Nilsen GK, Munthe-Kaas AZ, Skaug HJ, Brun M. Epistemic uncertainty quantification in deep learning classification by the Delta method. *Neural Netw*. 2022;145:164-176.
11. Abdar M, Samami M, Dehghani Mahmoodabad S, et al. Uncertainty quantification in skin cancer classification using three-way decision-based Bayesian deep learning. *Comput Biol Med*. 2021;135:104418.
12. Qin Y, Liu Z, Liu C, Li Y, Zeng X, Ye C. Super-resolved q-space deep learning with uncertainty quantification. *Med Image Anal*. 2021;67:101885.
13. Rahaman R. Uncertainty quantification and deep ensembles. *Adv Neural Inf Process Syst*. 2021;34.
14. Abdar M, Fahami MA, Chakrabarti S, et al. BARF: a new direct and cross-based binary residual feature fusion with uncertainty-aware module for medical image classification. *Inform Sci*. 2021;577:353-378.
15. Senousy Z, Abdelsamea MM, Gaber MM, et al. Mcua: multi-level context and uncertainty aware dynamic deep ensemble for breast cancer histology image classification. *IEEE Trans Biomed Eng*. 2021;69:818-829.
16. Abdar M, Salari S, Qahremani S, et al. UncertaintyFuseNet: robust uncertainty-aware hierarchical feature fusion model with ensemble Monte Carlo dropout for COVID-19 detection. *Image Video Process*. 2022;arXiv Preprint arXiv:2105.08590.
17. Barata C, Celebi ME, Marques JS. Development of a clinically oriented system for melanoma diagnosis. *Pattern Recognit*. 2017;69:270-285.
18. Badrinarayanan V, Handa A, Cipolla R. Segnet: a deep convolutional encoder-decoder architecture for robust semantic pixel-wise labelling. *Comput Vision Pattern Recognit*. 2015;arXiv Preprint arXiv:1505.07293.
19. Bi L, Kim J, Ahn E, Feng D, Fulham M. Semi-automatic skin lesion segmentation via fully convolutional networks. Paper presented at: 2017 IEEE 14th International Symposium on Biomedical Imaging (ISBI 2017); 2017:561-564. IEEE.
20. Alquran H, Qasmieh IA, Alqudah AM, et al. The melanoma skin cancer detection and classification using support vector machine. Paper presented at 2017 IEEE Jordan Conference on Applied Electrical Engineering and Computing Technologies (AEECT); 2017:1-5. IEEE.
21. Khan MA, Khan MA, Ahmed F, et al. Gastrointestinal diseases segmentation and classification based on duo-deep architectures. *Pattern Recognit Lett*. 2020;131:193-204.
22. Codella NC, Nguyen QB, Pankanti S, et al. Deep learning ensembles for melanoma recognition in dermoscopy images. *IBM J Res Dev*. 2017;61(4/5):5:1-5.
23. Daghrir J, Tlig L, Bouchouicha M, Sayadi M. Melanoma skin cancer detection using deep learning and classical machine learning techniques: a hybrid approach. Paper presented at: 2020 5th International Conference on Advanced Technologies for Signal and Image Processing (ATSIP); 2020:1-5. IEEE.
24. Bama S, Velumani R, Prakash N, Hemalakshmi G, Mohanarathinam A. Automatic segmentation of melanoma using superpixel region growing technique. *Mater Today Proc*. 2021;45:1726-1732.
25. Hu K, Niu X, Liu S, et al. Classification of melanoma based on feature similarity measurement for codebook learning in the bag-of-features model. *Biomed Signal Process Control*. 2019;51:200-209.
26. Ameri A. A deep learning approach to skin cancer detection in Dermoscopy images. *J Biomed Phys Eng*. 2020;10(6):801.
27. Jojoa Acosta MF, Caballero Tovar LY, Garcia-Zapirain MB, Percybrooks WS. Melanoma diagnosis using deep learning techniques on dermatoscopic images. *BMC Med Imaging*. 2021;21(1):1-11.
28. Zhang L, Yang G, Ye X. Automatic skin lesion segmentation by coupling deep fully convolutional networks and shallow network with textons. *J Med Imaging*. 2019;6(2):024001.
29. Shan P, Wang Y, Fu C, Song W, Chen J. Automatic skin lesion segmentation based on FC-DPN. *Comput Biol Med*. 2020;123:103762.
30. Bi L, Kim J, Ahn E, Kumar A, Feng D, Fulham M. Step-wise integration of deep class-specific learning for dermoscopic image segmentation. *Pattern Recognit*. 2019;85:78-89.
31. Adegun AA, Viriri S. Deep learning-based system for automatic melanoma detection. *IEEE Access*. 2019;8:7160-7172.
32. Nawaz M, Mehmood Z, Nazir T, et al. Skin cancer detection from dermoscopic images using deep learning and fuzzy k-means clustering. *Microsc Res Tech*. 2022;85(1):339-351.
33. Nawaz M, Masood M, Javed A, et al. Melanoma localization and classification through faster region-based convolutional neural network and SVM. *Multimedia Tools Appl*. 2021;80:1-22.
34. Banerjee S, Singh SK, Chakraborty A, Das A, Bag R. Melanoma diagnosis using deep learning and fuzzy logic. *Diagnostics*. 2020;10(8):577.
35. Iqbal I, Younus M, Walayat K, Kakar MU, Ma J. Automated multi-class classification of skin lesions through deep convolutional neural network with dermoscopic images. *Comput Med Imaging Graph*. 2021;88:101843.
36. Khan MA, Akram T, Zhang Y-D, Sharif M. Attributes based skin lesion detection and recognition: a mask RCNN and transfer learning-based deep learning framework. *Pattern Recognit Lett*. 2021;143:58-66.
37. Mohakud R, Dash R. Skin cancer image segmentation utilizing a novel EN-GWO based hyper-parameter optimized FCEDN. *J King Saud Univ Comput Inf Sci*. 2022.
38. Abdar M, Samami M, Mahmoodabad SD, et al. Uncertainty quantification in skin cancer classification using three-way decision-based Bayesian deep learning. *Comput Biol Med*. 2021;135:104418.
39. Pacheco AG, Krohling RA. An attention-based mechanism to combine images and metadata in deep learning models applied to skin cancer classification. *IEEE J Biomed Health Inform*. 2021;25(9):3554-3563.
40. Wang Y, Wang S. Skin lesion segmentation with attention-based SC-Conv U-net and feature map distortion. *Signal Image Video Process*. 2022;1-9.
41. Zhao C, Shuai R, Ma L, Liu W, Wu M. Segmentation of skin lesions image based on U-net++. *Multimedia Tools Appl*. 2022;81(6):8691-8717.

42. Durgarao N, Sudhavani G. Diagnosing skin cancer via C-means segmentation with enhanced fuzzy optimization. *IET Image Process.* 2021;15(10):2266-2280.
43. Haggenmüller S, Maron RC, Hekler A, et al. Skin cancer classification via convolutional neural networks: systematic review of studies involving human experts. *Eur J Cancer.* 2021;156:202-216.
44. Ali MS, Miah MS, Haque J, Rahman MM, Islam MK. An enhanced technique of skin cancer classification using deep convolutional neural network with transfer learning models. *Mach Learn Appl.* 2021;5:100036.
45. Polesel A, Ramponi G, Mathews VJ. Image enhancement via adaptive unsharp masking. *IEEE Trans Image Process.* 2000;9(3):505-510.
46. Muthukrishnan R, Radha M. Edge detection techniques for image segmentation. *Int J Comput Sci Inf Technol.* 2011;3(6):259-267.
47. Al-Amri SS, Kalyankar N, Khamitkar S. Image segmentation by using edge detection. *Int J Comput Sci Eng.* 2010;2(3):804-807.
48. Raja SK, KHADIR ASABDUL, Ahamed SR. Moving toward region-based image segmentation techniques: a study. *J Theor Appl Inf Technol.* 2009;5(1).
49. Kumar MJ, Kumar DGR, Reddy RVK. Review on image segmentation techniques. *Int J Sci Res Eng Technol.* 2014;2278-2882.
50. Zaitoun NM, Aqel MJ. Survey on image segmentation techniques. *Procedia Comput Sci.* 2015;65:797-806.
51. Albahli S, Nawaz M, Javed A, Irtaza A. An improved faster-RCNN model for handwritten character recognition. *Arab J Sci Eng.* 2021;46:1-15.
52. Albahli S, Nazir T, Irtaza A, Javed A. Recognition and detection of diabetic retinopathy using Densenet-65 based faster-RCNN. *Comput Mater Contin.* 2021;67:1333-1351.
53. Curiel-Lewandrowski C, Novoa RA, Berry E, et al. Artificial intelligence approach in melanoma. *Melanoma.* 2019;1-31.
54. Yuan Y. Automatic skin lesion segmentation with fully convolutional-deconvolutional networks. *Comput Vision Pattern Recognit.* 2017; arXiv Preprint arXiv:05165.
55. Berseth M. ISIC 2017-skin lesion analysis towards melanoma detection. *Comput Vision Pattern Recognit.* 2017; arXiv Preprint arXiv:00523.
56. Bi L, Kim J, Ahn E, Feng D. Automatic skin lesion analysis using large-scale dermoscopy images and deep residual networks. *Comput Vision Pattern Recognit.* 2017; arXiv Preprint arXiv:04197.
57. Menegola A, Tavares J, Fornaciali M, Li LT, Avila S, Valle E. RECOD titans at ISIC challenge 2017. *Comput Vision Pattern Recognit.* 2017; arXiv Preprint arXiv:04819.
58. Kawahara J, Hamarneh G. Fully convolutional neural networks to detect clinical dermoscopic features. *IEEE J Biomed Health Inf.* 2018;23(2):578-585.
59. Chowdary GJ, Yathisha G. Exploring dual-attention mechanism with multi-scale feature extraction scheme for skin lesion segmentation. *Image Video Process.* 2021; arXiv Preprint arXiv:08708.
60. Pravitasari AA, Iriawan N, Almuhyar M, et al. UNet-VGG16 with transfer learning for MRI-based brain tumor segmentation. *Telkomnika.* 2020;18(3):1310-1318.
61. Chu Z, Tian T, Feng R, Wang L. Sea-land segmentation with Res-UNet and fully connected CRF. Paper presented at: IGARSS 2019–2019 IEEE International Geoscience and Remote Sensing Symposium; 2019:3840-3843: IEEE.
62. Wibowo A, Purnama SR, Wirawan PW, Rasyidi H. Lightweight encoder-decoder model for automatic skin lesion segmentation. *Inf Med Unlocked.* 2021;100640.
63. Li X, Chen H, Qi X, Dou Q, Fu C-W, Heng P-A. H-DenseUNet: hybrid densely connected UNet for liver and tumor segmentation from CT volumes. *IEEE Trans Med Imaging.* 2018;37(12):2663-2674.
64. Nguyen DK, Tran TT, Nguyen CP, Pham VT. Skin lesion segmentation based on integrating EfficientNet and residual block into U-net neural network. Paper presented at: 2020 5th International Conference on Green Technology and Sustainable Development (GTSD); 2020:366-371. IEEE.
65. Gu R, Wang L, Zhang L. DE-net: a deep edge network with boundary information for automatic skin lesion segmentation. *Neurocomputing.* 2022;468:71-84.
66. Wu H, Chen S, Chen G, Wang W, Lei B, Wen Z. FAT-net: feature adaptive transformers for automated skin lesion segmentation. *Med Image Anal.* 2022;76:102327.
67. Banerjee S, Singh SK, Chakraborty A, Basu S, Das A, Bag R. Diagnosis of melanoma lesion using neutrosophic and deep learning. *Traitement du Signal.* 2021;38(5).
68. Khoulood S, Ahlem M, Fadel T, Amel S. W-net and inception residual network for skin lesion segmentation and classification. *Appl Intell.* 2021;52:1-19.
69. Hasan MK, Elahi MTE, Alam MA, Jawad MT, Martí R. DermoExpert: skin lesion classification using a hybrid convolutional neural network through segmentation, transfer learning, and augmentation. *Inf Med Unlocked.* 2022;100819.
70. Dai D, Dong C, Xu S, et al. Ms RED: a novel multi-scale residual encoding and decoding network for skin lesion segmentation. *Med Image Anal.* 2022;75:102293.
71. Kaur R, GholamHosseini H, Sinha R. Skin lesion segmentation using an improved framework of encoder-decoder based convolutional neural network. *Int J Imaging Syst Technol.* 2022.
72. Ramadan R, Aly S. CU-net: a new improved multi-input color U-net model for skin lesion semantic segmentation. *IEEE Access.* 2022;10:15539-15564.
73. Araújo RL, de Araújo FH, Silva RR. Automatic segmentation of melanoma skin cancer using transfer learning and fine-tuning. *Multimedia Syst.* 2021;1-12.
74. Dos Santos ES et al. Semi-automatic segmentation of skin lesions based on superpixels and hybrid texture information. *Med Image Anal.* 2022;77:102363.
75. Badshah N, Ahmad A. ResBCU-net: deep learning approach for segmentation of skin images. *Biomed Signal Process Control.* 2022;71:103137.

**How to cite this article:** Nawaz M, Nazir T, Masood M, et al. Melanoma segmentation: A framework of improved DenseNet77 and UNET convolutional neural network. *Int J Imaging Syst Technol.* 2022;1-17. doi:10.1002/ima.22750